

## Article

# The Facile Synthesis of Nickel-Doped Composite Magnetic Ni@CoO@ZIF-67 as an Efficient Heterogeneous Catalyst for the Ring-Opening Polymerization of L-Lactide

Xingxing Chen <sup>1,2</sup>, Qing Wu <sup>1,2</sup>, Somboon Chaemchuen <sup>1,3,\*</sup>  and Francis Verpoort <sup>1,4,5,\*</sup> 

<sup>1</sup> State Key Laboratory of Advanced Technology for Materials Synthesis and Processing, Wuhan University of Technology, Wuhan 430070, China; chenxingxing001117@163.com (X.C.); wu\_qing@whut.edu.cn (Q.W.)

<sup>2</sup> School of Materials Science and Engineering, Wuhan University of Technology, Wuhan 430070, China

<sup>3</sup> Department of Chemical Engineering, Faculty of Engineering, Mahidol University, Nakhon Pathom 73170, Thailand

<sup>4</sup> Research School of Chemical and Biomedical Technologies, National Research Tomsk Polytechnic University, Lenin Avenue 30, 634050 Tomsk, Russia

<sup>5</sup> Joint Institute of Chemical Research (FFMiEN), Peoples Friendship University of Russia (RUDN University), 6 Miklukho-Maklaya Str., 117198 Moscow, Russia

\* Correspondence: sama\_che@hotmail.com (S.C.); francis@whut.edu.cn (F.V.)

**Abstract:** The ring-opening polymerization of L-lactide is a crucial route for producing biodegradable polylactides (PLAs). Developing an efficient catalyst for this process poses significant challenges. Herein, we report the successful incorporation of nickel during the crystallization of ZIF-67, the derivation of the abundant and stable CoO source, to obtain the composite magnetic Ni@CoO@ZIF-67 using the solid-state thermal (SST) method. The characterization of the resulting materials revealed that nickel atoms are well dispersed in the composite CoO@ZIF-67, imparting additional magnetic properties. The composite Ni@CoO@ZIF-67 demonstrated superior performance as a heterogeneous catalyst for the ring-opening polymerization of L-lactide compared to reference materials such as Ni-Hmim, CoO, ZIF-67, and CoO@ZIF-67. Furthermore, the magnetic property of Ni@CoO@ZIF-67 offers practical advantages, enabling easier separation and recycling of the catalyst. Notably, the SST method facilitates the single-step synthesis of composite magnetic Ni@CoO@ZIF-67 under solvent-free conditions, representing a significant advancement in catalyst development. This approach not only simplifies the synthesis process but also inspires further developments of heterogeneous magnetic catalysts for a variety of effective and diverse reactions.

**Keywords:** zeolitic imidazole frameworks; solid-state thermal method; solvent-free synthesis; ring-opening polymerization; polylactic acid; bioplastic material



**Citation:** Chen, X.; Wu, Q.; Chaemchuen, S.; Verpoort, F. The Facile Synthesis of Nickel-Doped Composite Magnetic Ni@CoO@ZIF-67 as an Efficient Heterogeneous Catalyst for the Ring-Opening Polymerization of L-Lactide. *Catalysts* **2024**, *14*, 490. <https://doi.org/10.3390/catal14080490>

Academic Editor: Moris Eisen

Received: 1 July 2024

Revised: 22 July 2024

Accepted: 25 July 2024

Published: 30 July 2024



**Copyright:** © 2024 by the authors. Licensee MDPI, Basel, Switzerland. This article is an open access article distributed under the terms and conditions of the Creative Commons Attribution (CC BY) license (<https://creativecommons.org/licenses/by/4.0/>).

## 1. Introduction

Plastic or polymeric materials have become increasingly popular and are commonly used in modern life. These materials are typically produced from petroleum-based sources, which are non-renewable and have a significant environmental impact. The production process of plastic materials requires a large amount of energy and contributes to carbon emissions. Additionally, plastic waste takes hundreds or thousands of years to degrade, leading to severe environmental pollution [1]. Therefore, bioplastic or biopolymer materials offer a more sustainable alternative to traditional plastic materials. Bioplastics are derived from bio-based sources and are biodegradable in natural environments. One example of a bioplastic material is polylactic acid (PLA), produced from lactic acid or lactide monomer. PLA can be used in various applications such as drug delivery, packaging, compost bags, and other environmentally friendly products [2–4]. One of the advantages of the PLA (polylactic acid) polymer is its hydrolytic degradation, which is primarily due to its renewable origin [5–7]. PLA can be broken down by microorganisms such as fungi or bacteria under

natural conditions. This characteristic renders PLA products bioassimilable, making them green and environmentally friendly materials.

The synthesis of PLA can be achieved by directly converting the lactic acid monomer into a polymer through polycondensation. However, this method typically results in a low-molecular-weight PLA product. An alternative and more practical approach is the ring-opening polymerization (ROP) of lactide, which yields high-molecular-weight PLA products. In the ROP mechanism, the catalyst plays a crucial role in converting the lactide monomer into high-molecular-weight PLA through internal transesterification [8,9]. Stannous octoate and tin (II) chloride are commonly used catalysts for ROP [10,11]. The organo-Sn(II) is the most widely used complex for the industrial preparation of PLA. However, many other active catalysts (e.g., Zn, Ln, Al, Y, and alkaline earth metals) are also used for LA polymerization [12–14]. However, these catalysts are homogeneous, meaning they are dissolved and mixed in the solution, resulting in non-recyclability or complicated recycling processes. Heterogeneous catalysts, which have different phases in the reaction, offer greater environmental and economic benefits. However, the development of heterogeneous catalysts for ROP has been rarely reported in the literature [15,16].

Among the heterogeneous catalysts, metal–organic frameworks (MOFs) or zeolitic imidazole frameworks (ZIFs) have recently been proposed as efficient heterogeneous catalysts for PLA synthesis from L-lactide [17–22]. Their high density of metal ions in the uniform framework of organic ligands provides bi-functional acidic and base active sites for the ROP reaction. For example, ZIF-8, based on zinc ions and 2-methyl imidazole ligands, has been applied as a heterogeneous catalyst for the polymerization of L-Lactide to cyclic poly(lactide) [17,18,22]. The Lewis acid deriving from open zinc sites initiates monomer (LA) propagation. Meanwhile, the basic sites deriving from the imidazole ligand promote zinc alkoxide formation to facilitate chain growth, eventually undergoing intramolecular transesterification to release cyclic polylactide and liberate a free catalyst. Moreover, catalysts related to metal–organic frameworks (MOFs), Porous organic polymers (POPs), or Covalent organic frameworks (COFs) have been applied for the polymerization and copolymerization of various cyclic esters [23–26].

Zeolitic imidazole frameworks (ZIFs) belong to a new class of materials known as metal–organic frameworks (MOFs). These materials are formed when organic imidazole ligands coordinate with metal ions or clusters to create ordered frameworks in two or three dimensions. However, the ZIFs are classified as having a unique name from MOFs due to their structure, which is analogous to the zeolite structure topology. The unique framework structure of ZIFs, a mixed structure of an MOF and a zeolite, results in diverse compositions and properties. Additionally, the large porosity and stability of ZIFs provide a high potential for diverse applications [27,28]. Moreover, post-synthetic modification (PSM) with different components can be carried out to modify properties and thus further extend the applications of ZIFs.

The solvothermal method is a traditional method for synthesizing ZIFs. Initially, the metal and ligand source are dissolved in the organic solvent, followed by thermal treatment for a specified period. Although the organic solvent can be replaced by water or the synthesis can be conducted at room temperature, this method has evolved to accommodate various solvent-free techniques. These include mechanochemical, ball-milling, and thermal synthesis from metal oxides. However, challenges such as solvent waste formation, post-processing treatment, high energy consumption, and time requirements hinder the scalable and large-scale synthesis of ZIFs. Thus, a facile and green synthesis route is essential for the practical and industrial-scale production of ZIFs.

Recently, a solvent-free synthesis method known as the in situ thermal (IST) or solid-state thermal (SST) method has been reported. This method enables the direct use of synthesized ZIFs for further applications without the need for post-treatment or activation [24,29,30]. The SST method successfully produced ZIF-8 (zinc-based) and ZIF-67 (cobalt-based) frameworks. Additionally, iron (III) atoms were incorporated into crystalline ZIF-67 (Fe@ZIF-67) through the SST method to create hybridized Fe/Co ZIF-67. This

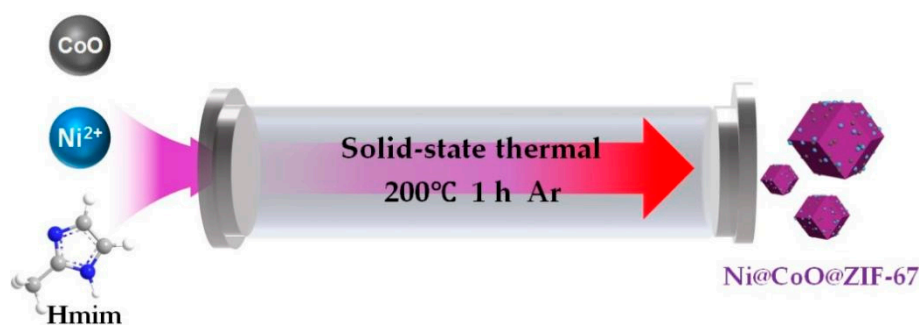
hybridization improved the chemical properties and significantly enhanced the catalytic activity for CO<sub>2</sub> fixation compared to monocobalt ion-based ZIF-67. Inspired by previous reports on different metal complex catalysts for ring-opening polymerization (ROP), the nickel complex has shown high potential as a homogeneous catalyst for PLA synthesis among various metal complexes [31–33].

In this study, a simple method for incorporating nickel into a composite magnetic material named Ni@CoO@ZIF-67 was developed. This strategy involved a single-step, solvent-free process using the SST method, presenting an innovative approach to synthesizing composite magnetic materials. Different ratios of nickel to cobalt (x) in the precursor were used to create Ni<sub>x</sub>@CoO@ZIF-67. The impact of nickel content on the structure and properties was studied using various analytical techniques. The resulting Ni<sub>x</sub>@CoO@ZIF-67 was then used as a catalyst for the ring-opening polymerization (ROP) of polylactic acid (PLA). The magnetic properties of the optimal Ni<sub>10</sub>@CoO@ZIF-67 catalyst allowed for easy separation and recycling using an external magnet, with no significant decrease in catalytic efficiency for at least five cycles. It is important to note that having an abundant and stable source of CoO was beneficial for creating the crystalline ZIF-67 and achieving the desired magnetic properties in the Ni@CoO@ZIF-67 catalyst. Additionally, the incorporation of nickel significantly improved the catalytic performance of ROP in synthesizing PLA.

## 2. Results and Discussion

### 2.1. Material Synthesis and Characterization

The straightforward solid-state thermal (SST) method was employed to synthesize Ni-doped composite magnetic Ni@CoO@ZIF-67. The key strategy of the SST method involves the thermal treatment of a solid precursor composed of mixed metals (Co and Ni) and Hmim ligand sources. The precursor undergoes thermal treatment at a mild temperature of 200 °C under solvent-free conditions (Scheme 1). The abundant and stable structure of the CoO source is utilized to form ZIF-67, contributing to the composite's magnetic properties from unreacted CoO. Meanwhile, Ni is simultaneously incorporated into the structure during the crystallization of the composite materials.



**Scheme 1.** The solid-state thermal method (SST) used to synthesize Ni@CoO@ZIF-67.

This facile, single-step synthesis method requires no post-treatment or activation, offering advantages over other solvent-free methods. The SST method eliminates waste organic solvents, reduces energy consumption due to its low-temperature operation, and shortens synthesis duration. Additionally, the solvent-free approach overcomes the limitations of metal source solubility, enabling high metal loading. The SST method's simplicity and efficiency hold high potential for the scalable synthesis and large-scale production of composite materials.

The nickel-free CoO@ZIF-67 was initially synthesized following the procedure described in previous reports [24]. The diffraction pattern of CoO@ZIF-67 exhibited mixed diffraction peaks of ZIF-67 and CoO patterns (Figures 1a and S1), confirming the successful synthesis of composite magnetic CoO@ZIF-67 using the SST method. Following this, various nickel sources (nickel (II) acetylacetonate) with different ratios (x: 5, 10, 20, 30, and 50% mol based on CoO) were introduced into the synthetic precursor to obtain Ni<sub>x</sub>@CoO@ZIF-

67. The diffraction peaks of CoO at  $36.5^\circ$ ,  $42.4^\circ$ ,  $61.5^\circ$ , and  $73.7^\circ$ , corresponding to the crystal planes (111), (200), (220), and (311), respectively (JCPDS 43-1004), were observed in all Ni ratios of the synthesized materials. The presence of CoO diffraction indicated that unreacted CoO was maintained and composited in all synthesized  $\text{Ni}_x\text{CoO@ZIF-67}$  samples.

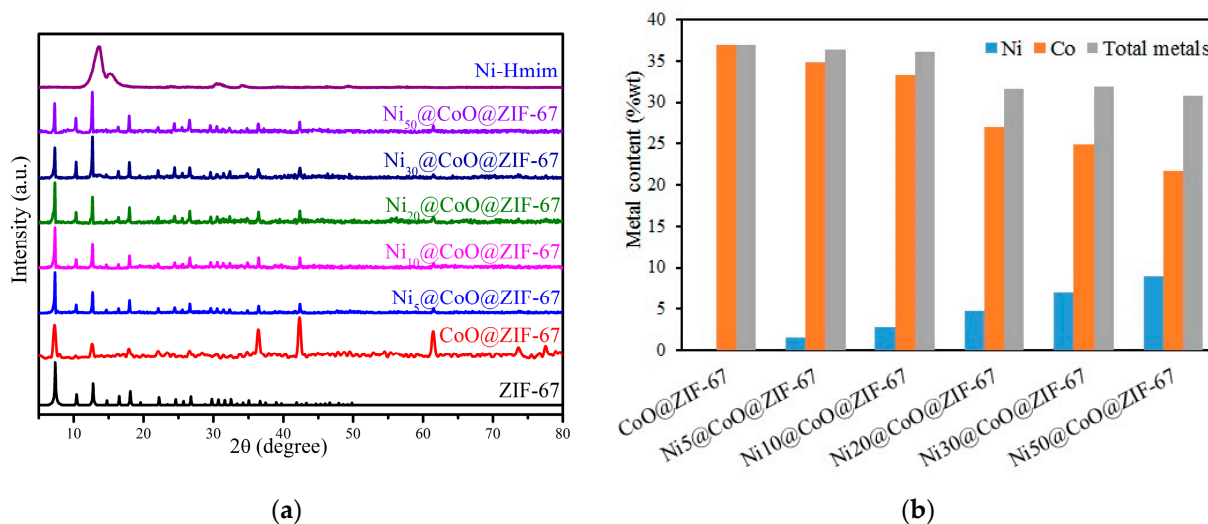


**Figure 1.** (a) Diffraction patterns of  $\text{Ni}_x\text{CoO@ZIF-67}$ , ZIF-67, CoO@ZIF-67, and Ni-Hmim. (b) The metal content measured by ICP-OES in  $\text{Ni}_x\text{CoO@ZIF-67}$ .

Additionally, the characteristic crystal planes (001), (002), (112), (022), (013), and (222) of ZIF-67 were clearly observed for different Ni ratios in  $\text{Ni}_x\text{CoO@ZIF-67}$  [34,35]. However, the peak ratios of the diffractive ZIF-67 pattern appeared to be slightly different for the 30% and 50% Ni ratios (Ni<sub>30</sub>@CoO@ZIF-67 and Ni<sub>50</sub>@CoO@ZIF-67). In comparison, the nickel source mixed with Hmim under the SST method, denoted as Ni-Hmim, displayed a broad peak in its diffraction pattern, which did not match the diffraction patterns of CoO@ZIF-67 and  $\text{Ni}_x\text{CoO@ZIF-67}$ . Notably, the diffraction intensity of Ni-Hmim was much weaker, indicating a smaller crystal size compared to other synthesized materials. Due to its small crystal size, further characterization of Ni-Hmim, such as single crystal analysis, was not feasible.

The XRD results indicate that Ni was incorporated into the crystal structure of  $\text{Ni}_x\text{CoO@ZIF-67}$  at specific nickel ratios. At low Ni ratios (<30% Ni based on CoO), the addition of Ni had an insignificant effect on crystallization. However, at higher Ni ratios (>30% Ni), an excess of Ni interfered with crystal formation, similar to the effect observed with ZIF-67 under the SST method. Replacing the cobalt source with a nickel source mixed with Hmim under the SST method produced a different diffraction pattern (Ni-Hmim). These diffraction patterns suggest that Co and Ni exhibit distinct coordination behaviors with the imidazole ligand during material formation.

The metal content in the synthesized materials was determined using Inductively Coupled Plasma Optical Emission Spectroscopy (ICP-OES). During the synthesis of  $\text{Ni}_x\text{CoO@ZIF-67}$ , it was observed that the cobalt content decreased as the Ni ratios in the mixed precursor increased (Figure 1b). Conversely, the nickel content in  $\text{Ni}_x\text{CoO@ZIF-67}$  exhibited an increasing trend. Notably, a higher Ni ratio led to a decrease in the total metal content of  $\text{Ni}_x\text{CoO@ZIF-67}$ . At high Ni ratios, the Ni ions competed to coordinate with Hmim to form a complex like Ni-Hmim or Ni-(Hmim)<sub>y</sub>, where y is 1–4 molecules of Hmim, without growing a framework. The crystallization decreased with higher Ni ratios, as evidenced by the decreasing intensity of XRD (Figure 1a). The complex Ni-Hmim formation and decreased crystallization resulted in a diluted total metal content in the synthesized materials.

In the synthesis process of  $\text{Ni}_x\text{@CoO@ZIF-67}$ , an excess ratio of imidazole (Hmim) to CoO (6:1) was used in the mixed precursor, which exceeds the theoretical formula of ZIF-67 (2:1). Throughout the synthesis of different  $\text{Ni}_x\text{@CoO@ZIF-67}$  samples, the cobalt source (CoO) in the precursor remained constant. The results suggested that the imidazole linker coordinated with additional Ni, resulting in a more extensive M-ligand (M: Co, Ni) framework. Therefore, the metal content analysis (ICP-OES) indicated that both cobalt and nickel ions promoted metal coordination with the imidazole ligand during the synthesis of  $\text{Ni}_x\text{@CoO@ZIF-67}$ .

The framework of ZIFs is formed by a metal-coordinated imidazole ligand, which provides variable pore space and a large surface area, resulting in unique porosity properties. Using the SST method, CoO reacted with Hmim to produce the porous material  $\text{CoO@ZIF-67}$ , as previously reported [24]. In this study, varying nickel content was incorporated into the structure of  $\text{Ni}_x\text{@CoO@ZIF-67}$ , affecting its porosity and surface area, which were determined by  $\text{N}_2$  adsorption at 77 K.

The  $\text{N}_2$  adsorption isotherm revealed sharp  $\text{N}_2$  adsorption at low pressures ( $P/P_0 < 0.05$ ), indicating a predominant micropore structure (Isotherm type I) in  $\text{Ni}_x\text{@CoO@ZIF-67}$  (Figure 2). In contrast, Ni-Hmim showed significant  $\text{N}_2$  adsorption at high relative pressures ( $P/P_0 > 0.85$ ). The specific surface area was calculated from  $\text{N}_2$  adsorption at 77 K. It was found that the specific surface area remained relatively unchanged with Ni incorporation from 5% to 20% in  $\text{CoO@ZIF-67}$ , as summarized in Table 1. However, the surface area slightly decreased with an over 30% Ni ratio ( $\text{Ni}_{30}\text{@CoO@ZIF-67}$  and  $\text{Ni}_{50}\text{@CoO@ZIF-67}$ ). A very low surface area ( $107 \text{ m}^2/\text{g}$ ) was observed when Co was completely replaced with Ni in the synthetic precursor (Ni-Hmim).

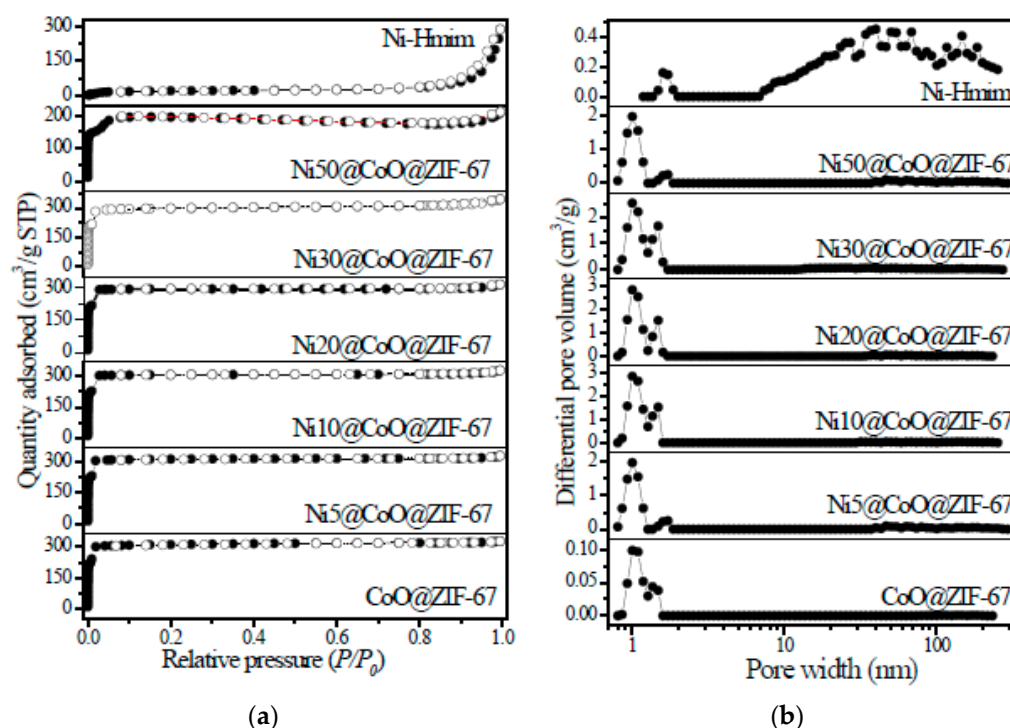


**Figure 2.** (a)  $\text{N}_2$  adsorption isotherms and (b) the DFT pore size distribution of  $\text{Ni}_x\text{@CoO@ZIF-67}$ ,  $\text{CoO@ZIF-67}$ , and Ni-Hmim.

The decreased surface area at high Ni ratios (30–50% Ni ratio) was correlated with the reduced pore volume and pore size (Table 1). The DFT pore size distribution further confirmed the presence of micropores in  $\text{Ni}_x\text{@CoO@ZIF-67}$  (pore size < 2 nm), as shown in Figure 2b. In contrast, the pore size distribution of Ni-Hmim indicated that the material predominantly contained large pores (>10 nm) with a slight mixture of micropores.

**Table 1.** The specific surface area and porosity properties of the synthesized materials.

Material	Surface Area (m <sup>2</sup> /g)		Pore Volume <sup>1</sup> (cm <sup>3</sup> /g)	Pore Size <sup>1</sup> (nm)
	BET	Langmuir		
CoO@ZIF-67	1353	1432	0.48	1.25
Ni5@CoO@ZIF-67	1351	1437	0.48	1.25
Ni10@CoO@ZIF-67	1367	1440	0.47	1.25
Ni20@CoO@ZIF-67	1312	1399	0.45	1.25
Ni30@CoO@ZIF-67	1290	1371	0.46	1.25
Ni50@CoO@ZIF-67	753	797	0.30	1.23
Ni-Hmim	107	124	0.03	2.17

<sup>1</sup> Pore volume and pore size were calculated from the HK method.

The morphology of the nickel composite magnetic Ni@CoO@ZIF-67 was examined using scanning electron microscopy (SEM) and transmission electron microscopy (TEM). Among the synthesized Ni<sub>x</sub>@CoO@ZIF-67 samples, Ni<sub>10</sub>@CoO@ZIF-67 exhibited the best catalytic performance. Therefore, the impact of nickel integration on the structure was investigated by comparing Ni<sub>10</sub>@CoO@ZIF-67 with CoO@ZIF-67.

SEM images of Ni<sub>10</sub>@CoO@ZIF-67 revealed a non-uniform shape (Figure 3b). Typically, the SST method for synthesizing ZIF-67 and CoO@ZIF-67 results in a rhombic dodecahedral shape (Figure 3a). The irregular shape of Ni<sub>10</sub>@CoO@ZIF-67 suggests the influence of competing coordination between cobalt ions and nickel ions in bonding with Hmim during the SST method. The solvent-free conditions and short synthesis process in the SST method resulted in the imperfect crystallization of Ni<sub>10</sub>@CoO@ZIF-67. Additionally, TEM provided a more detailed understanding of the structure, shape, and elemental dispersion of Ni<sub>10</sub>@CoO@ZIF-67. A combination of CoO particles (dark spots) was observed within the Ni<sub>10</sub>@CoO@ZIF-67 particles, with crystalline ZIF-67 covering the CoO particles (Figure 3c). Elemental mapping revealed that nickel was homogeneously dispersed along with cobalt within the ZIF-67 framework (Figure 3d–g). The TEM images suggest that nickel and cobalt were well-dispersed, with nanoparticle CoO composites embedded in the Ni<sub>10</sub>@CoO@ZIF-67.

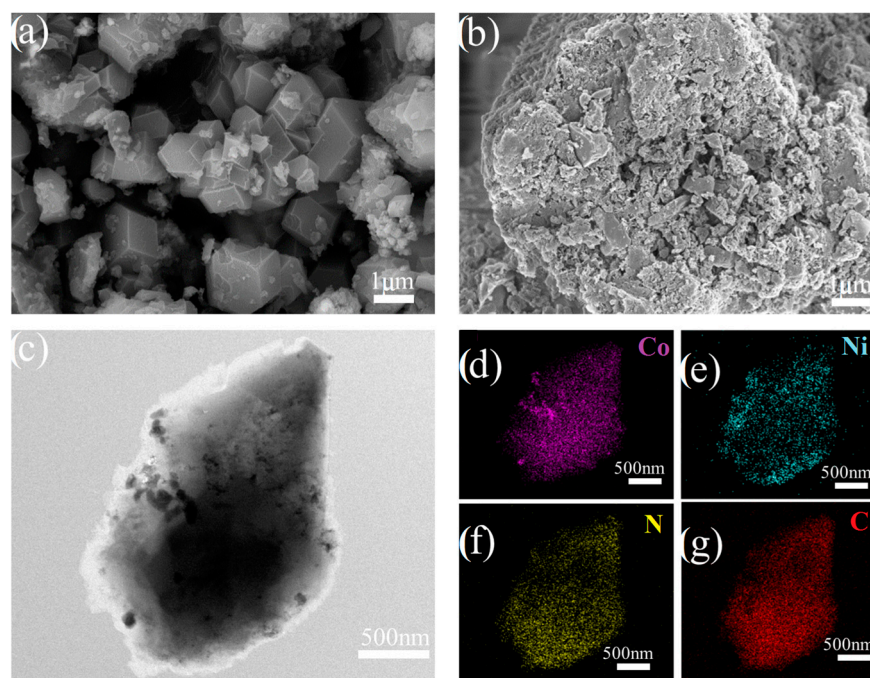


**Figure 3.** SEM Images of CoO@ZIF-67 (a) and Ni<sub>10</sub>@CoO@ZIF-67 (b), TEM images (c), and elemental mapping of Ni<sub>10</sub>@CoO@ZIF-67 on cobalt (d), nickel (e), nitrogen (f), and carbon (g).

To study the chemical coordination of functional groups in the synthesized materials, Fourier transform infrared (FTIR) spectroscopy was performed. The FTIR spectra for Ni10@CoO@ZIF-67 and CoO@ZIF-67 were similar, as shown in Figure S2. The spectra exhibited stretching and bending vibrations of the imidazole ligand [36]. Peaks at  $1456\text{--}1410\text{ cm}^{-1}$  and  $1300\text{--}992\text{ cm}^{-1}$  corresponded to the stretching vibrations of the C=N and C-N bonds, respectively. Peaks at  $750\text{--}690\text{ cm}^{-1}$  indicated the bending vibration of the C-N bond of 2-methylimidazole. The adsorption signal of the M-N bond (M: Co or Ni) was observed at  $425\text{ cm}^{-1}$  [37]. Additionally, the stretching vibration peaks of the Co=O bond at  $561\text{ cm}^{-1}$  and  $659\text{ cm}^{-1}$  further confirmed the presence of CoO in the materials. Broad spectral bands at  $3300\text{--}3600\text{ cm}^{-1}$  indicated the stretching vibration of  $\text{--OH}$  in  $\text{H}_2\text{O}$  molecules [38]. These IR spectra confirm the formation of ZIF-67 and the partial adsorption of  $\text{H}_2\text{O}$  molecules, aligning well with the XRD results.

The elemental composition and electronic valence states of the materials were further investigated using X-ray photoelectron spectroscopy (XPS). The survey spectra revealed common peaks corresponding to Co 2p, N 1s, C 1s, and O 1s for both Ni10@CoO@ZIF-67 and CoO@ZIF-67 (Figure 4a). Additionally, the presence of the Ni 2p peak exclusively in Ni10@CoO@ZIF-67 indicated successful Ni incorporation (Figure 4b). To further analyze the chemical state of each element, the high-resolution spectra of each element were compared between Ni10@CoO@ZIF-67 and CoO@ZIF-67. The Co 2p spectra were deconvoluted into Co 2p<sub>3/2</sub> with a peak at 781.2 eV, a satellite peak at 786.4 eV, and Co 2p<sub>1/2</sub> with a peak at 796.7 eV and a satellite peak at 802.4 eV (Figure 4c) [36,39]. These peaks were assigned to the  $\text{Co}^{2+}$  species in the synthesized materials, indicating that the nickel incorporation did not influence the chemical state of the cobalt species.

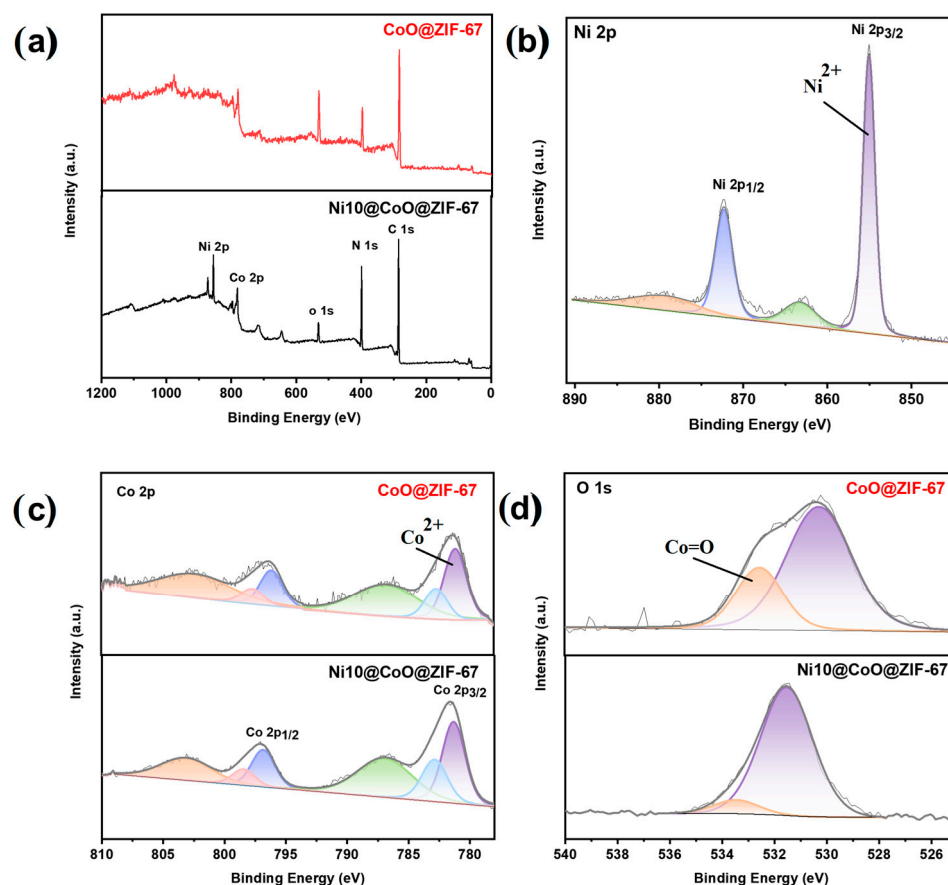


**Figure 4.** XPS Spectra of the composite magnetic Ni10@CoO@ZIF-67 compared to CoO@ZIF-67, (a) survey spectra, (b) Ni 2p, (c) Co2p, and (d) O1s.

For the oxygen element, the binding energies were deconvoluted into spin states of O 1s, with distinct peaks at 533.3 eV and 531.3 eV. The peak at 533.3 eV represented the presence of  $O^{2-}$  originating from CoO, which was significantly reduced in Ni10@CoO@ZIF-67 compared to CoO@ZIF-67. This reduction suggests that the surface of Ni10@CoO@ZIF-67 contained less CoO than CoO@ZIF-67, implying that more CoO in the precursor was converted in Ni10@CoO@ZIF-67.

Nickel incorporation was confirmed by the binding energies of the Ni 2p spectra (Figure 4d). The Ni10@CoO@ZIF-67 showed characteristic peaks of Ni 2p<sub>3/2</sub> at 854.8 eV and Ni 2p<sub>1/2</sub> at 872.1 eV, indicating the presence of Ni<sup>2+</sup> [37,40]. It is important to note that the nickel source used in the synthetic precursor was Ni<sup>2+</sup>, validating that the state of Ni was maintained during the SST method.

The CoO source provided a bifunctional precursor, serving both as the cobalt source for the formation of ZIF-67 and as a composite material to impart magnetic properties to Ni@CoO@ZIF-67. The magnetization of the materials was measured using a vibrating sample magnetometer (VSM). The magnetization curve revealed a highly symmetrical curve without a hysteresis loop, passing through the zero point (Figure 5). The coercivity and remanence were approximately zero, indicating that the materials exhibited superparamagnetism.

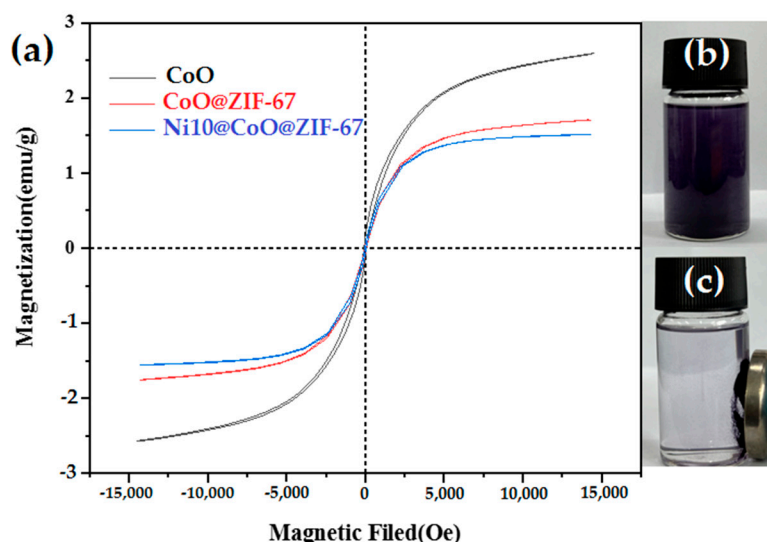


**Figure 5.** (a) VSM curves of CoO, CoO@ZIF-67, and Ni10@CoO@ZIF-67. (b) Images of catalyst dispersion, and (c) the external magnet to separate the Ni10@CoO@ZIF-67 from the reaction mixture.

However, the incorporation of Ni led to a significant decrease in saturation magnetization: from 2.58 emu/g for CoO to 1.67 emu/g for CoO@ZIF-67, and further to 1.67 emu/g for Ni10@CoO@ZIF-67. The weaker magnetization is likely due to the sacrificial conversion of CoO (a magnetic material) to coordinate with Hmim, forming ZIF-67. Additionally, the introduction of Ni promoted the formation of metal–ligand bonds (Co–N and Ni–N), which further diluted the magnetic strength of Ni10@CoO@ZIF-67. Nevertheless, the magnetization of Ni10@CoO@ZIF-67 was still sufficient to enable easy separation from a mixed solution after an applied reaction using an external magnet.

## 2.2. Ring-Opening Polymerization of L-Lactide

The synthesized materials were applied as heterogeneous catalysts for the ring-opening polymerization (ROP) of L-lactide (LA). Under similar reaction conditions, the incorporated Ni catalyst demonstrated an improvement in catalytic performance compared to the non-nickel functionalized catalyst (CoO@ZIF-67), as shown in Figure 6a. Specifically, Ni10@CoO@ZIF-67 exhibited the highest catalytic conversion of LA at 90%, which is approximately 20% higher than that of CoO@ZIF-67. However, further increasing the Ni



content in the catalysts (Ni20@CoO@ZIF-67, Ni30@CoO@ZIF-67) did not result in a significant change in catalytic performance, and a decrease in conversion was observed with the highest Ni content catalyst (Ni50@CoO@ZIF-67). Meanwhile, the Ni-Hmim catalyst, which replaced cobalt with nickel in the synthetic precursor, resulted in the lowest conversion of LA (40%) under similar reaction conditions.

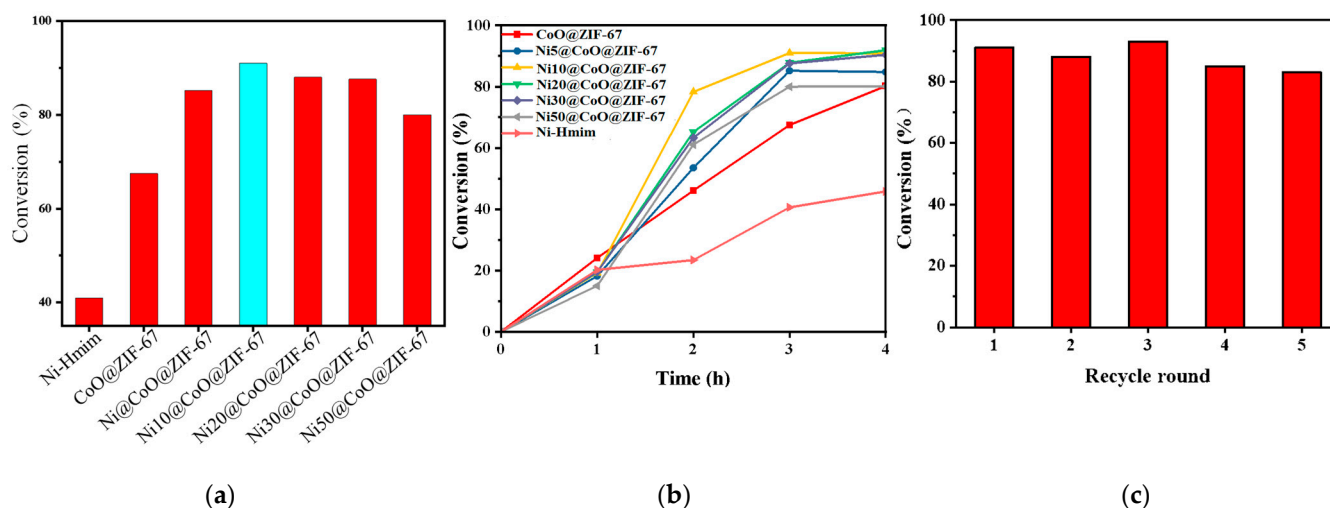


**Figure 6.** (a) The catalytic comparison for L-lactide conversion, (b) the kinetic study of different catalysts, and (c) the catalytic performance of the recycled Ni10@CoO@ZIF-67 catalyst. Reaction conditions entailed 4 mg of catalyst, monomer/catalyst ratio (M/C) of 100/1, reaction temperature of 160 °C for 3 h.

Additionally, the kinetic study of the chemical reaction was elucidated by performing reactions at different times (Figure 6b). Initially, after 1 h, CoO@ZIF-67 exhibited slightly better catalytic performance among the synthesized catalysts. However, the Ni-incorporated catalysts showed a marked improvement in catalytic activity after 2 h compared to CoO@ZIF-67 and Ni-Hmim catalysts. The Ni50@CoO@ZIF-67 catalyst achieved the highest conversion of LA after a reaction time of 3 h. In contrast, the Ni5@CoO@ZIF-67 and Ni20@CoO@ZIF-67 catalysts required an extended reaction time of 4 h to achieve high conversion, similar to Ni10@CoO@ZIF-67. Ni30@CoO@ZIF-67, Ni50@CoO@ZIF-67, and CoO@ZIF-67 required significantly longer times to reach maximum conversion. The Ni-Hmim catalyst exhibited the lowest catalytic rate among the synthesized catalysts.

Furthermore, the formation of macrocyclic PLA showed that the number average molecular weight ( $M_n$ ) values and polydispersity (PDI) for CoO@ZIF-67 and Ni10@CoO@ZIF-67 catalysts were insignificantly different ( $M_n$ : 17.04 and 17.41 kg/mol and PDI: 1.86 and 1.71, respectively), as shown in Figures S5 and S6. These results indicate that incorporating Ni into the composite magnetic Ni@CoO@ZIF-67 catalysts enhances the catalysts' reactivity for the ROP of LA. The synergistic effect of Ni and Co, along with high metal dispersion on a large surface area catalyst, is proposed to contribute to the excellent performance of Ni10@CoO@ZIF-67 in catalyzing L-lactide polymerization.

The recycling ability of a catalyst to maintain catalytic performance is a crucial characteristic of heterogeneous catalysts. Given its excellent performance, the Ni10@CoO@ZIF-67 catalyst was further tested to determine its recycling ability for the ring-opening polymerization (ROP) of L-lactide (LA). Utilizing the composite magnetic nature of the catalyst, an external magnet was employed to separate the Ni10@CoO@ZIF-67 catalyst from the reaction mixture. To remove any residual compounds (such as LA or PLA) that might be trapped in the catalyst's pores, dichloromethane (DCM) was used as a solvent. The DCM was replaced 3-4 times, and the catalyst was then dried in a vacuum oven at 80 °C overnight.

The reused Ni10@CoO@ZIF-67 catalyst was subjected to the ROP of LA under identical conditions: 4 mg of catalyst, a monomer-to-catalyst ratio (M/C) of 100:1, and a reaction

temperature of 160 °C for 3 h. The results demonstrated that the Ni10@CoO@ZIF-67 catalyst could be recycled while maintaining a high conversion rate of LA for at least five cycles (Figure 6c). Despite minor variations in LA conversion that were less than 5% in each cycle, these fluctuations suggest an insignificant change in the catalytic activity of Ni10@CoO@ZIF-67. The minor variations in conversion could be attributed to the residual trapping of LA, PLA, or solvent within the catalyst's pores, affecting the catalyst's weight in each cycle.

The excellent recyclability of the Ni10@CoO@ZIF-67 catalyst was further characterized using various techniques. The crystal structure of the reused catalyst was examined using X-ray diffraction (XRD). The diffraction pattern of the reused Ni10@CoO@ZIF-67 catalyst was compared with that of the fresh catalyst, as shown in Figure S3. The reused catalyst exhibited a diffraction pattern similar to the fresh catalyst, although a decrease in crystallinity or peak intensity was observed. This reduction in crystallinity is likely due to the agglomeration and coverage of residual compounds (e.g., LA, PLA) on the surface or within the pores of the catalyst.

The chemical state of the elements in the catalyst was analyzed using X-ray photoelectron spectroscopy (XPS). The survey spectra indicated a similar elemental composition in both the fresh and reused Ni10@CoO@ZIF-67 catalysts (Figure S4a). The deconvoluted spectra of the Ni 2p region showed that the Ni species remained consistent in both fresh and reused catalysts (Figure S4b), confirming that nickel was chemically coordinated within the structure of the Ni10@CoO@ZIF-67 catalyst. High-resolution spectra of the Co 2p region also showed similar spectra for both fresh and reused catalysts (Figure S4c), indicating that the chemical states of cobalt and nickel remained unchanged after the reaction.

However, some changes were observed in the oxygen spectrum of the reused catalyst compared to the fresh one (Figure S4d). The O 1s peak at 533.3 eV showed increased intensity in the reused catalysts. This increase may be attributed to the exposure and subsequent washing of CoO and uncovered (non-magnetic) ZIFs with the organic solvent DCM during the recycling process. Despite this change in the oxygen spectrum, it did not significantly affect the reactivity of the catalyst, which maintained excellent catalytic performance for at least five cycles.

In summary, the chemical environment of the Ni10@CoO@ZIF-67 catalyst remained relatively stable after the reaction, reflecting the overall stability of this heterogeneous catalyst. This stability, combined with its high catalytic performance and effective recyclability, underscores the potential of Ni10@CoO@ZIF-67 for practical applications in industrial processes.

### 3. Materials and Methods

#### 3.1. Chemicals and Catalyst Synthesis

All chemicals and solvents used for the synthesis of catalysts and the ring-opening polymerization (ROP) of polylactic acid (PLA) were purchased from Shanghai Aladdin Chemical Company (Shanghai, China). The purity of the chemicals was of an analytical grade (AR), and they were used directly without any further purification or extraction. The cobalt (II) oxide (CoO) is commercial, purchased from Shanghai Aladdin Chemical Company (Shanghai, China), and directly used without further purification or extraction. The powder CoO was non-uniform at the micro-scale (10–100 μm).

**Nix@CoO@ZIF-67:** The Nix@CoO@ZIF-67 was synthesized using a modified solid-state thermal (SST) method based on previously reported procedures [20]. The process involved physically mixing cobalt oxide (CoO, 1 mmol) and 2-methylimidazole (Hmim, 6 mmol) with different amounts of nickel (II) acetylacetonate (x of Ni(acac): 5, 10, 20, 30, and 50% mol based on CoO) in a mortar under solvent-free conditions. The uniformly mixed solid precursor was then transferred into a ceramic boat and placed into a tubular furnace (TL 1200, Nanjing Bo Yun Tong Instrument Technology Co. Ltd., Nanjing, China).

The precursor in the furnace was purged with an argon flow of 50 cc/min for 5 min before the thermal treatment. The thermal treatment was controlled with a programmable

temperature profile: the temperature was ramped from room temperature to 100 °C within 30 min, and then to 200 °C within 20 min. The sample was held at 200 °C for 60 min before naturally cooling to room temperature. The resulting products (referred to as NiX@CoO@ZIF-67) were used directly for catalytic applications or characterization without requiring additional post-purification or activation. Notably, the NiX@CoO@ZIF-67 could be stored in dry conditions to prevent water adsorption.

**Ni-Hmim:** A similar SST method was applied to synthesize Ni-Hmim, with the modification of replacing CoO with nickel (II) acetylacetonate (1 mmol), which was mixed with 2-methylimidazole (6 mmol). After proceeding with the SST method, the obtained product was denoted as Ni-Hmim.

### 3.2. Characterization

The crystalline structure of the synthesized materials was determined using powder X-ray diffraction (PXRD) with a Bruker D8 Advance diffractometer (Billerica, MA, USA) in Bragg–Brentano geometry. The instrument was operated at 40 kV and 45 mA with Cu K $\alpha$  radiation, and the scan rate was set at 0.1° per second over an angular range of 5° to 80°. The morphology of the materials was investigated using Scanning Electron Microscopy (SEM) on a JEOL JSM-5610LV instrument (Akishima, Japan), operated in the range of 0.5–35 kV, and High-Resolution Transmission Electron Microscopy (HRTEM) on a JEOL JEM-2100 instrument with an electron beam energy of 200 kV. The chemical bonding and functional groups were analyzed using Fourier-transform infrared (FT-IR) spectroscopy with a Bruker Vertex 80 V spectrometer. X-ray photoelectron spectroscopy (XPS) was conducted using a Thermo Fischer ESCALAB 250Xi spectrometer (Waltham, MA, USA). The adventitious carbon located at 284.8 eV was used to calibrate the samples. The porosity and surface area of the materials were measured using a Micromeritics ASAP 2020 instrument (Norcross, GA, USA), with samples activated at 200 °C under a dynamic vacuum for 200 min before measuring N<sub>2</sub> adsorption at 77 K. Thermal stability was assessed using thermogravimetric analysis (TGA) with a NETZSCH STA-449C simultaneous TG-DTA apparatus (Selb, Germany), heating at a rate of 10 °C/min under a flowing air atmosphere at 50 cc/min. Magnetic properties were characterized using a Superconducting Quantum Interference Device-Vibrating Sample Magnetometer (SQUID-VSM) instrument (Quantum Design GmbH, Pfungstadt, Germany). The qualitative and quantitative examination of the elemental composition was performed using an Inductively Coupled Plasma Optical Emission Spectrometer (ICP-OES) manufactured by Agilent (Santa Clara, CA, USA).

### 3.3. ROP for Synthesis PLA

The synthesized NiX@CoO@ZIF-67 was directly applied as a catalyst for the ring-opening polymerization (ROP) to synthesize polylactic acid (PLA). The NiX@CoO@ZIF-67 catalysts (4 mg) and L-Lactide (L-LA, 260 mg) were mixed in a molar ratio of 100/1 (monomer/catalyst) and transferred into a 10 mL high-pressure glass tube in a glove box under an argon (Ar) atmosphere. The reactor containing the solid mixture (catalyst and L-LA), filled with inert Ar gas and free from oxygen and solvent, was transferred to a pre-heated oven set at 160 °C for a specific reaction time. After cooling to room temperature, the obtained crude polymer was dried under a vacuum. The conversion rate of the monomer was determined by <sup>1</sup>H NMR spectroscopy (CDCl<sub>3</sub>) (integration of methine resonances at  $\delta$  = 5.05 ppm for the monomer vs.  $\delta$  = 5.16 ppm for the polymer).

To terminate the reaction, the reactor was quenched in cold water, and then placed in a refrigerator at 5 °C for 3 h before further processing. A large amount of dichloromethane (DCM) was added to the reactor to dissolve the polymer. The catalyst was then recovered for recycling by centrifugation (9000 rpm, 3 min) and washed with fresh DCM four times before being dried at 80 °C in a vacuum oven. This dried catalyst is referred to as the reused catalyst.

#### 4. Conclusions

A facile method was reported to incorporate Ni into composite magnetic Ni@CoO@ZIF-67-6 through the solid-state thermal method (SST). The different Ni incorporation that affected the structure and properties of materials was verified using several analysis techniques. The iso-structure and properties as no-nickel incorporation were obtained at a low Ni ratio (<30%Ni ratio based on the cobalt source). The Ni ions were homogeneously well dispersed in the composite magnetic Ni@CoO@ZIF-67. However, the high induced Ni ratio (>30% Ni ratio) interfered with the crystal formation and the properties of the obtained materials. Further, the series of the Ni incorporation on Ni<sub>x</sub>@CoO@ZIF-67 was applied to catalyze the ring-opening polymerization of L-lactide to synthesize PLA. The Ni-functionalized catalyst significantly improved the catalytic performance of the applied reaction. The Ni incorporation suggests exposing more active sites and thus, more available sites to initiate the ring-opening of the LA monomer. Among the synthesized materials, Ni<sub>10</sub>@CoO@ZIF-67 exhibited the highest catalytic activity under comparable conditions. Additionally, the Ni<sub>10</sub>@CoO@ZIF-67-6 catalyst maintained its high catalytic activity over at least five cycles, facilitated by simple separation using an external magnet.

**Supplementary Materials:** The following supporting information can be downloaded at: <https://www.mdpi.com/article/10.3390/catal14080490/s1>, Figure S1. XRD spectra of Hmim, CoO, CoO@ZIF-67, and ZIF-67; Figure S2. FTIR spectra of Ni<sub>10</sub>@CoO@ZIF-67 and CoO@ZIF-67; Figure S3. XRD spectra of fresh and reused Ni<sub>10</sub>@CoO@ZIF-67 catalyst; Figure S4. XPS Spectra of fresh Ni@CoO@ZIF-67 compared to reused Ni@CoO@ZIF-67 catalyst; Figure S5. Mn value using the CoO@ZIF-67 catalyst, Notably the reaction condition entailed 4 mg of catalyst, a monomer/catalyst ratio (M/C) of 100/1, and a reaction temperature was 160 °C for 3 h; Figure S6. Mn value using Ni<sub>10</sub>@CoO@ZIF-67 catalyst, Notable: reaction condition of 4 mg of catalyst, monomer/catalyst ratio (M/C) of 100/1, reaction temperature of 160 °C for 3 h; Figure S7. TEM images of elemental mapping on Ni<sub>10</sub>@CoO@ZIF-67: (a) carbon, (b) nitrogen, (c) nickel, (d) cobalt; and Table S1. Precursor amount to the synthesis of Ni<sub>x</sub>@CoO@ZIF-67 catalysts.

**Author Contributions:** Conceptualization, X.C. and S.C.; methodology, X.C.; formal analysis, Q.W.; investigation, X.C. and Q.W.; data curation, X.C. and Q.W.; writing—original draft preparation, X.C. and Q.W.; writing—review and editing, S.C.; supervision, S.C. and F.V.; project administration, F.V.; funding acquisition, S.C. and F.V. All authors have read and agreed to the published version of the manuscript.

**Funding:** The authors are grateful to the State Key Lab of Advanced Technology for Materials Synthesis and Processing for financial support (Wuhan University of Technology).

**Data Availability Statement:** Data are contained within the article and Supplementary Materials.

**Conflicts of Interest:** The authors declare no conflicts of interest.

#### References

1. Ali, A.; Bahadar, A.; Khan, A.; Sanaullah, K. Role of agricultural waste in recycled plastic biocomposites. In *Recycled Plastic Biocomposites*; Elsevier: Amsterdam, The Netherlands, 2022; pp. 165–194.
2. Taib, N.-A.A.B.; Rahman, M.R.; Huda, D.; Kuok, K.K.; Hamdan, S.; Bakri, M.K.B.; Julaihi, M.R.M.B.; Khan, A. A review on poly lactic acid (PLA) as a biodegradable polymer. *Polym. Bull.* **2023**, *80*, 1179–1213. [[CrossRef](#)]
3. Farah, S.; Anderson, D.G.; Langer, R. Physical and mechanical properties of PLA, and their functions in widespread applications—A comprehensive review. *Adv. Drug Delivery Rev.* **2016**, *107*, 367–392. [[CrossRef](#)] [[PubMed](#)]
4. McKeown, P.; Jones, M.D. The chemical recycling of PLA: A review. *Sustain. Chem.* **2020**, *1*, 1–22. [[CrossRef](#)]
5. Torres, A.; Li, S.; Roussos, S. Poly(lactic acid) degradation in soil or under controlled conditions. *J. Appl. Polym. Sci.* **1996**, *62*, 2295–2302. [[CrossRef](#)]
6. Li, S.; Girard, A.; Garreau, H.; Vert, M. Enzymatic degradation of polylactide stereocopolymers with predominant D-lactyl contents. *Polym. Degrad. Stab.* **2000**, *71*, 61–67. [[CrossRef](#)]
7. Bubpachat, T.; Sombatsompop, N.; Prapagdee, B. Isolation and role of polylactic acid-degrading bacteria on degrading enzymes productions and PLA biodegradability at mesophilic conditions. *Polym. Degrad. Stab.* **2018**, *152*, 75–85. [[CrossRef](#)]
8. Nampoothiri, K.M.; Nair, N.R.; John, R.P. An overview of the recent developments in polylactide (PLA) research. *Bioresour. Technol.* **2010**, *101*, 8493–8501. [[CrossRef](#)]

9. Masutani, K.; Kimura, Y. PLA synthesis. From the monomer to the polymer. In *Poly(lactic acid) Science and Technology: Processing, Properties, Additives and Applications*; The Royal Society of Chemistry: London, UK, 2014.
10. Lee, E.J.; Lee, K.M.; Jang, J.; Kim, E.; Chung, J.S.; Do, Y.; Yoon, S.C.; Park, S.Y. Characteristics of silica-supported tin(II) methoxide catalysts for ring-opening polymerization (ROP) of L-lactide. *J. Mol. Catal. A Chem.* **2014**, *385*, 68–72. [[CrossRef](#)]
11. Kang, M.-S.; Cho, J.; Nayab, S.; Jeong, J.H. Synthesis and characterization of Zn(II) and Cu(II) complexes bearing (chiral substituent)(diethyl)-ethanediamine derivatives as precatalysts for rac-lactide polymerisation. *Polyhedron* **2019**, *158*, 135–143. [[CrossRef](#)]
12. Punyodom, W.; Meepowpan, P.; Girdthep, S.; Limwanich, W. Influence of tin (II), aluminum (III) and titanium (IV) catalysts on the transesterification of poly (L-lactic acid). *Polym. Bull.* **2022**, *79*, 11409–11429. [[CrossRef](#)]
13. McGuire, T.M.; Buchard, A.; Williams, C. Chemical Recycling of Commercial Poly (l-lactic acid) to l-Lactide Using a High-Performance Sn (II)/Alcohol Catalyst System. *J. Am. Chem. Soc.* **2023**, *145*, 19840–19848. [[CrossRef](#)] [[PubMed](#)]
14. Gao, C.; Wang, Y.; Yang, Y.; Qin, S. Poly (lactic acid) synthesized from non-food biomass feedstocks with tin-loaded ZA molecular sieve catalysts by direct melt polycondensation. *Polym. Int.* **2024**, *73*, 310–318. [[CrossRef](#)]
15. Wanna, N.; Kraithong, T.; Khamnaen, T.; Phiriyawirut, P.; Charoenchaidet, S.; Tantirungrotechai, J. Aluminum-and calcium-incorporated MCM-41-type silica as supports for the immobilization of titanium (IV) isopropoxide in ring-opening polymerization of l-lactide and  $\epsilon$ -caprolactone. *Catal. Commun.* **2014**, *45*, 118–123. [[CrossRef](#)]
16. Jones, M.D.; Davidson, M.G.; Keir, C.G.; Hughes, L.M.; Mahon, M.F.; Apperley, D.C. *Zinc (II) Homogeneous and Heterogeneous Species and Their Application for the Ring-Opening Polymerisation of rac-Lactide*; Wiley Online Library: Hoboken, NJ, USA, 2009.
17. Luo, Z.; Chaemchuen, S.; Zhou, K.; Verpoort, F. Ring-Opening Polymerization of l-Lactide to Cyclic Poly (Lactide) by Zeolitic Imidazole Framework ZIF-8 Catalyst. *ChemSusChem* **2017**, *10*, 4135–4139. [[CrossRef](#)] [[PubMed](#)]
18. Chaemchuen, S.; Dai, Q.; Wang, J.; Zhu, C.; Klomkliang, N.; Yuan, Y.; Cheng, C.; Elkadi, M.; Luo, Z.; Verpoort, F. Enhancing catalytic activity via metal tuning of zeolitic imidazole frameworks for ring opening polymerization of l-lactide. *Appl. Catal. A* **2021**, *624*, 118319. [[CrossRef](#)]
19. Naz, F.; Mousavi, B.; Luo, Z.; Jabbour, C.; Heynderickx, P.M.; Chaemchuen, S.; Verpoort, F. Switching from linear to cyclic  $\delta$ -Polyvalerolactone synthesized via zeolitic imidazolate framework as a catalyst: A promising approach. *Appl. Organomet. Chem.* **2019**, *33*, e4890. [[CrossRef](#)]
20. Abdur, R.M.; Mousavi, B.; Shahadat, H.M.; Akther, N.; Luo, Z.; Zhuiykov, S.; Verpoort, F. Ring-opening copolymerization of  $\epsilon$ -caprolactone and  $\delta$ -valerolactone by a titanium-based metal–organic framework. *New J. Chem.* **2021**, *45*, 11313–11316. [[CrossRef](#)]
21. Luo, Z.; Chaemchuen, S.; Zhou, K.; Gonzalez, A.A.; Verpoort, F. Influence of lactic acid on the catalytic performance of MDABCO for ring-opening polymerization of L-lactide. *Appl. Catal. A* **2017**, *546*, 15–21. [[CrossRef](#)]
22. Chaemchuen, S.; Luo, Z.; Zhou, K.; Mousavi, B.; Phatanasri, S.; Jaroniec, M.; Verpoort, F. Defect formation in metal–organic frameworks initiated by the crystal growth-rate and effect on catalytic performance. *J. Catal.* **2017**, *354*, 84–91. [[CrossRef](#)]
23. Liu, Y.; Ren, Z.; Zhang, N.; Yang, X.; Wu, Q.; Cheng, Z.; Xing, H.; Bai, Y. A nanoscale MOF-based heterogeneous catalytic system for the polymerization of N-carboxyanhydrides enables direct routes toward both polypeptides and related hybrid materials. *Nat. Commun.* **2023**, *14*, 5598. [[CrossRef](#)]
24. Chaemchuen, S.; Wu, Q.; Gu, J.-F.; Yuan, Y.; Klomkliang, N.; Verpoort, F. Solvent-Free Synthesis of Composite Magnetic CoO@ZIF-67 for Efficient and Practical Use. *Microporous Mesoporous Mater.* **2024**, *376*, 113200. [[CrossRef](#)]
25. Zhao, J.; Guo, G.; Wang, D.; Liu, H.; Zhang, Z.; Sun, L.; Ding, N.; Li, Z.; Zhao, Y. A “one-step” approach to the highly efficient synthesis of lactide through the confinement catalysis of covalent organic frameworks. *Green Chem.* **2023**, *25*, 3103–3110. [[CrossRef](#)]
26. Debruyne, M.; Van Speybroeck, V.; Van Der Voort, P.; Stevens, C.V. Porous organic polymers as metal free heterogeneous organocatalysts. *Green Chem.* **2021**, *23*, 7361–7434. [[CrossRef](#)]
27. Chaemchuen, S.; Zhou, K.; Mousavi, B.; Ghadamyari, M.; Heynderickx, P.M.; Zhuiykov, S.; Yusubov, M.S.; Verpoort, F. Spray drying of zeolitic imidazolate frameworks: Investigation of crystal formation and properties. *CrystEngComm* **2018**, *20*, 3601–3608. [[CrossRef](#)]
28. Sun, Y.; Zhang, N.; Yue, Y.; Xiao, J.; Huang, X.; Ishag, A. Recent advances in the application of zeolitic imidazolate frameworks (ZIFs) in environmental remediation: A review. *Environ. Sci. Nano* **2022**, *9*, 4069–4092. [[CrossRef](#)]
29. Wang, J.; Chaemchuen, S.; Klomkliang, N.; Verpoort, F. In situ thermal solvent-free synthesis of zeolitic imidazolate frameworks with high crystallinity and porosity for effective adsorption and catalytic applications. *Cryst. Growth Des.* **2021**, *21*, 5349–5359. [[CrossRef](#)]
30. Shi, G.; Xu, W.; Wang, J.; Klomkliang, N.; Mousavi, B.; Chaemchuen, S. Thermochemical transformation in the single-step synthesis of zeolitic imidazole frameworks under solvent-free conditions. *Dalton Trans.* **2020**, *49*, 2811–2818. [[CrossRef](#)] [[PubMed](#)]
31. Dutta, S.; Hung, W.-C.; Huang, B.-H.; Lin, C.-C. Recent developments in metal-catalyzed ring-opening polymerization of lactides and glycolides: Preparation of polylactides, polyglycolide, and poly (lactide-co-glycolide). *Synth. Biodegrad. Polym.* **2011**, *245*, 219–283.
32. John, A.; Katiyar, V.; Pang, K.; Shaikh, M.M.; Nanavati, H.; Ghosh, P. Ni (II) and Cu (II) complexes of phenoxy-ketimine ligands: Synthesis, structures and their utility in bulk ring-opening polymerization (ROP) of L-lactide. *Polyhedron* **2007**, *26*, 4033–4044. [[CrossRef](#)]
33. Sun, J.; Shi, W.; Chen, D.; Liang, C. The ring-opening polymerization of D,L-lactide catalyzed by new complexes of Cu, Zn, Co, and Ni Schiff base derived from salicylidene and L-aspartic acid. *J. Appl. Polym. Sci.* **2002**, *86*, 3312–3315. [[CrossRef](#)]

34. Banerjee, R.; Phan, A.; Wang, B.; Knobler, C.; Furukawa, H.; O’Keeffe, M.; Yaghi, O.M. High-throughput synthesis of zeolitic imidazolate frameworks and application to CO<sub>2</sub> capture. *Science* **2008**, *319*, 939–943. [[CrossRef](#)]
35. Wu, Q.; Gu, J.; Wang, J.; Liu, N.; Chaemchuen, S. Impact in rational synthesis Co-ZIF templates for derived the structural Co@NC catalysis for high efficient hydrogen and oxygen evolution reactions. *Int. J. Hydrogen Energy* **2023**, *48*, 2663–2676. [[CrossRef](#)]
36. Shi, S.; Liu, Z.; Miao, X.; Wang, C.; Liu, B.; Wang, G.; Jin, Z. Broad-spectrum absorptive ZnCr LDHs/ZIF-67 S-scheme heterojunction for hydrogen evolution reaction under visible irradiation. *J. Photochem. Photobiol. A* **2024**, *455*, 115768. [[CrossRef](#)]
37. Thamilselvan, A.; Dang, V.D.; Doong, R.-A. Ni-Co bimetallic decorated dodecahedral ZIF as an efficient catalyst for photo-electrochemical degradation of sulfamethoxazole coupled with hydrogen production. *Sci. Total Environ.* **2023**, *873*, 162208. [[CrossRef](#)]
38. Cheng, C.; Zhang, J.; Zeng, R.; Xing, F.; Huang, C. Schottky barrier tuning via surface plasmon and vacancies for enhanced photocatalytic H<sub>2</sub> evolution in seawater. *Appl. Catal. B* **2022**, *310*, 121321. [[CrossRef](#)]
39. Xie, H.; Wang, K.; Li, S.; Jin, Z. Construction of Co<sub>9</sub>S<sub>8</sub>/MoS<sub>2</sub>/Ni<sub>2</sub>P double S-scheme heterojunction for enhanced photocatalytic hydrogen evolution. *Surf. Interfaces* **2023**, *42*, 103353. [[CrossRef](#)]
40. Yue, X.; Dong, Y.; Cao, H.; Wei, X.; Zheng, Q.; Sun, W.; Lin, D. Effect of electronic structure modulation and layer spacing change of NiAl layered double hydroxide nanoflowers caused by cobalt doping on supercapacitor performance. *J. Colloid Interface Sci.* **2023**, *630*, 973–983. [[CrossRef](#)]

**Disclaimer/Publisher’s Note:** The statements, opinions and data contained in all publications are solely those of the individual author(s) and contributor(s) and not of MDPI and/or the editor(s). MDPI and/or the editor(s) disclaim responsibility for any injury to people or property resulting from any ideas, methods, instructions or products referred to in the content.